Molecular Therapy
Nucleic Acids
Original Article

Selection and Identification of Skeletal-Muscle-Targeted RNA Aptamers

Styliana Philippou,[1,4] Nikolaos P. Mastroyiannopoulos,[1,4] Neoklis Makrides,[2,4] Carsten W. Lederer,[3,4] Marina Kleanthous,[3,4] and Leonidas A. Phylactou[1,4]

[1]Department of Molecular Genetics, Function & Therapy, The Cyprus Institute of Neurology and Genetics, P.O. Box 23462, 1683 Nicosia, Cyprus; [2]Clinic A, Neuropathology Department, The Cyprus Institute of Neurology and Genetics, P.O. Box 23462, 1683 Nicosia, Cyprus; [3]Department of Molecular Genetics Thalassaemia, The Cyprus Institute of Neurology and Genetics, P.O. Box 23462, 1683 Nicosia, Cyprus; [4]The Cyprus School of Molecular Medicine, The Cyprus Institute of Neurology and Genetics, P.O. Box 23462, 1683 Nicosia, Cyprus

Oligonucleotide gene therapy has shown great promise for the treatment of muscular dystrophies. Nevertheless, the selective delivery to affected muscles has shown to be challenging because of their high representation in the body and the high complexity of their cell membranes. Current trials show loss of therapeutic molecules to non-target tissues leading to lower target efficacy. Therefore, strategies that increase uptake efficiency would be particularly compelling. To address this need, we applied a cell-internalization SELEX (Systematic Evolution of Ligands by Exponential Enrichment) approach and identified a skeletal muscle-specific RNA aptamer. A01B RNA aptamer preferentially internalizes in skeletal muscle cells and exhibits decreased affinity for off-target cells. Moreover, this *in vitro* selected aptamer retained its functionality *in vivo*, suggesting a potential new approach for targeting skeletal muscles. Ultimately, this will aid in the development of targeted oligonucleotide therapies against muscular dystrophies.

INTRODUCTION

Muscular dystrophies are a genetically heterogeneous group of more than 40 muscle disorders that are characterized by muscle weakness and wasting of the skeletal muscle.[1] Although their underlying cellular pathologies are diverse, almost all types of muscular dystrophies have one feature in common: they arise from single-gene mutations.[2] Therefore, the most promising approaches for treatment involve gene therapy either by the modification or replacement of a faulty gene with another functional healthy copy.[2] For Duchenne muscular dystrophy (DMD), for example, which is the most common form of muscular dystrophies, the disrupted reading frame of the dystrophin pre-mRNA can be restored by hybridizing antisense oligonucleotides (AONs) to the sense target sequence.[3] Clinical trials for exon 51 skipping have been tested with both the 2′-O-methyl phosphorothioate (2′-OMe PS) (Drisapersen) and phosphorodiamidate morpholino (PMO) (Eteplirsen) AON chemistry.[4–7] The latter has been approved by the US Food and Drug Administration (FDA) in September 2016 and is currently in ongoing clinical trials to confirm its efficacy.[8] Similarly, chemically modified AONs complementary to the CUG expanded repeat have been designed for Myotonic Dystrophy type 1 (DM1) to target the nuclear retained transcripts.[9–11] The limiting factor of current gene therapy approaches, common not only in these two muscular dystrophies but in all muscular dystrophies, is the low muscle cell selectivity leading to an unpredictable expression among several organs when administered systemically.[12,13] This undesirable biodistribution results in loss of a substantial amount of the therapeutic molecules, ultimately leading to lower target efficacy.[14] Furthermore, the use of higher starting doses to compensate for the loss leads to dose-dependent side effects such as toxicity and activation of immunological responses.[15] Therefore, by coupling the sequences with a target-specific vehicle, the tissue specificity during systemic delivery could be significantly improved.

Aptamers are a class of small, synthetic, single-stranded nucleic acids that fold into unique secondary structures.[16] They can be chemically modified with 2′-fluoropyrimidines (2′-F) to reduce their nuclease sensitivity, and unlike peptides and monoclonal antibodies, they are essentially non-immunogenic even when administered in excess amounts.[17–19] Aptamers are identified via Systematic Evolution of Ligands by Exponential Enrichment (commonly referred to as SELEX). This process involves a series of affinity purification and amplification rounds through which a large pool of random sequences is narrowed down to the most promising candidate aptamer sequences.[18,19]

Variations of the SELEX methodology such as Cell-SELEX, Cross-Over SELEX, and Tissue-SELEX have given the capability of binding numerous targets including organic compounds, nucleotides, proteins, and even whole cells and organisms.[19–22] Of particular interest is the more recent cell-internalization SELEX where aptamers can be selected to bind, internalize, and potentially deliver agents into cells. For example, in the work of Chu et al.,[23] silencing of gene expression was achieved by an anti-prostate-specific membrane antigen (PSMA)

Received 8 November 2017; accepted 6 December 2017;
https://doi.org/10.1016/j.omtn.2017.12.004.

Correspondence: Leonidas A. Phylactou, PhD, The Cyprus Institute of Neurology and Genetics, P.O. Box 23462, 1683 Nicosia, Cyprus.
E-mail: laphylac@cing.ac.cy

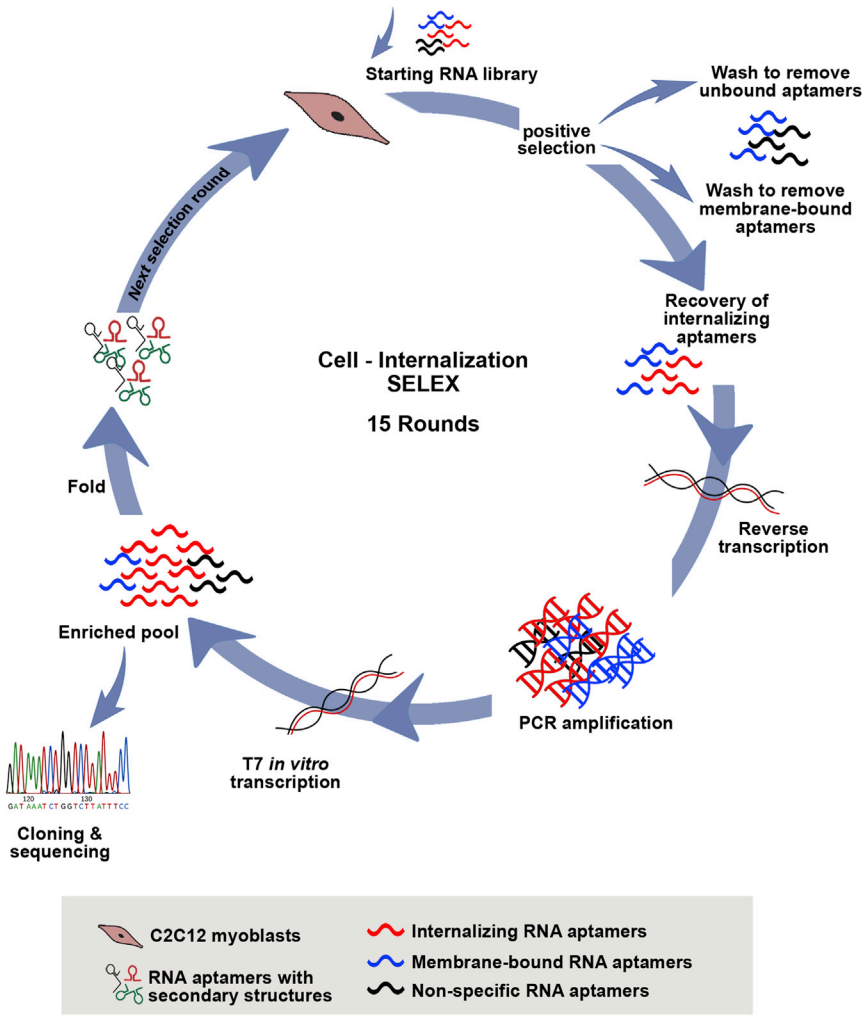

Figure 1. Aptamer Selection Strategy

Schematic representation of the evolution of internalizing RNA aptamers for skeletal muscle via 15 cell-internalization SELEX rounds. See also Figure S1. (Figure created by author from data in Figure 1 in RAPID-SELEX for RNA Aptamers, by Sveto et al., 2013, PLOS One.[92] © 2013 Szeto et al. Creative Commons Attribution License applies.)

RNA aptamer conjugated with a small interfering RNA (siRNA). Similarly to Cell-SELEX, specific cell-surface molecules or even unknown membrane receptors may be directly targeted within their native environment, allowing a straightforward enrichment of cell-specific aptamers.[24]

Our long-term goal is to identify aptamers that will selectively and efficiently internalize in several diseased muscles, and thus aid the delivery of therapeutic oligonucleotides in skeletal muscle. The ability of aptamers to bind to a specific target with extreme affinity and specificity makes them ideal candidates for targeted therapies.[25,26] Consequently, the aim of this study was the identification of the first RNA aptamer (A01B) that enters efficiently into skeletal muscle cells. Using cell-internalization SELEX, we identified one such aptamer that specifically binds to skeletal muscle cells and retains skeletal muscle internalization efficiency *in vivo* following local delivery. Therefore, this aptamer may prove a useful tool for improving the muscle specificity and internalization efficiency for a wide spectrum of therapeutic sequences. Ultimately, this will open a new era of safe and targeted aptamer-mediated therapies, which could benefit the broader group of muscular dystrophies.

RESULTS

In Vitro Selection of Skeletal Muscle Cell-Internalizing RNA Aptamers

An initial single-stranded DNA library was designed with a 40-nt-long random region between two fixed primer binding sites. The corresponding RNA transcripts were generated by *in vitro* transcription following incorporation of a T7 promoter sequence upstream of the sequence of interest (Figure S1). To improve stability and nuclease resistance of the transcripts, we also incorporated 2′-F pyrimidines during *in vitro* transcription. A cell-internalization SELEX protocol was next employed to identify 2′-F-modified RNA aptamers that selectively bind and internalize into skeletal muscle cells (Figure 1). For each selection round, the pool of random RNA sequences was selected against (positive selection) the target cell line, proliferating C2C12 muscle cells. A total of 15 such rounds was required to enrich the population with specific RNA sequences. For rounds 1–4, the selection conditions remained unchanged, whereas from round 6 onward the selective pressure was progressively increased by shortening the internalization time with the target and increasing the number and volume of washes (Table 1). At each round of selection, internalizing RNA aptamers were re-amplified to produce the enriched population for the next selection round. New 2′-F-modified RNA transcripts were generated as done previously (Figure S1).

Assessment of Aptamer Enrichment during *In Vitro* Selection

During the selection, additional experiments were performed to assess the level of enrichment and whether more stringent conditions were required to further increase enrichment. To achieve this, we studied an early, intermediate, and late round of selection (rounds 2, 10, and 15, respectively) throughout the experimental work flow. First, the complexity of the RNA pools at the selected rounds was assessed using a DNA melt curve analysis (Figures 2A and 2B).[27] As the double-stranded PCR products were heated incrementally, they dissociated at different temperatures depending on the pool

Table 1. Selection Conditions

		Blocking		Internalization		Cold Washes	
Rounds	RNA (pmol)	tRNA (μg/mL)	Time (min)	Cell Line	Time (min)	PBS (mL)	Salt Wash (mL)
1	1,500	100	15	C2C12	120	3 × 3	1 × 3
2	1,500	100	15	C2C12	120	3 × 3	1 × 3
3	1,500	100	15	C2C12	120	3 × 3	1 × 3
4	1,500	100	15	C2C12	120	3 × 3	1 × 3
5	1,500	100	15	C2C12	120	3 × 3	1 × 3
6	1,500	100	15	C2C12	120	3 × 5	1 × 5
7	1,500	100	15	C2C12	90	3 × 5	1 × 5
8	1,500	100	15	C2C12	90	3 × 5	1 × 5
9	1,500	100	15	C2C12	90	3 × 5	1 × 5
10	1,500	100	15	C2C12	60	3 × 5	1 × 5
11	1,500	100	15	C2C12	60	3 × 10	1 × 10
12	1,500	100	15	C2C12	60	3 × 10	1 × 10
13	1,500	100	15	C2C12	30	5 × 10	1 × 10
14	1,500	100	15	C2C12	30	5 × 10	1 × 10
15	1,500	100	15	C2C12	15	5 × 10	1 × 10

complexity. A significant drop in the library complexity was observed between rounds 2 and 10, as evidenced by the shift of the round 10 DNA melt curve toward higher temperatures (79.2°C). Interestingly, the DNA melt assay performed for round 15 showed minimal change in the library complexity as compared with round 10, indicating that no more rounds of selection were required. Another indication of the aforementioned result was the change in the curve's shape from short and wide at round 2 to high and narrow at rounds 10 and 15 (Figure 2A). Likewise, this was further confirmed by the shape of the dissociation curve, as shown in Figure 2B. More specifically, for round 2, a slight decrease followed by an increase in the slope between 65°C and 75°C was observed. This graphical shape is characteristic of a population of variable structural complexity that dissociates gradually. Although structural complexity was similar for rounds 10 and 15, an additional increase in the fluorescent signal was observed from the former to the latter, suggesting enrichment of specific aptamer sequences or structures in round 15 (Figure 2B). This enrichment in the pool population was next verified by measuring the levels of cell internalizing aptamers at the selected rounds. Internalization was evident from round 2 and continued to increase at a steady rate, with the RNA pool at round 15 being the most efficient (Figure 2C). These data are in agreement with the data from the DNA melt curve analysis and suggest that enrichment of specific aptamer sequences has indeed occurred in the pool population (Figure 2B). The enrichment process was also monitored by confocal microscopy using fluorescein-labeled aptamer pools. It was observed that when comparing the aptamer pool from round 2 with round 15, fluorescein levels in C2C12 cells increased significantly (Figure S2). In order to next assess the cellular localization of the aptamer pool at the final round (round 15), higher magnification confocal images were obtained. As illustrated in Figure 2D, the aptamer pool localizes into the cytoplasm of proliferating C2C12 cells. Taken together, all these data suggest that aptamer convergence has occurred and the selection should be terminated at round 15.

Identification of Skeletal Muscle Cell-Specific RNA Aptamers

RNA pools from the previously selected rounds were converted to cDNA, cloned, sequenced, and aligned to each other using different software packages in order to identify the dominating aptamer sequences (Figure 3A). First, the raw sequencing data were aligned to an input reference sequence which utilizes the known primer binding sites (Figure S1A). Once the correct sequences were identified and isolated from those that were either incomplete or incorrect, the individual clones were clustered into groups based on the alignment of their sequences. A total of seven unique aptamer sequences were identified throughout the selection (Figure 3B). Interestingly, after eight rounds of selection (from round 2 to round 10) the pool population evolved from being random to having preference (60% of the population) for a particular sequence (A01B) in round 10. In round 15, there was continuation of this sequence (48.72% of the total population) and increase of another sequence, A01D, that was also first identified in round 10 (Figure 3A). This drop in the frequency of the A01B sequence was due to the very short incubation time (15 min) that was used at round 15. By comparing this with the 60-min incubation time at round 10, we concluded that the drop is insignificant because a relatively high number of this particular sequence was able to internalize in such a short amount of time. Furthermore, the percentage of random sequences remained unchanged from round 10 (26.6%) to round 15 (24.35%), indicating that evolution of sequences is no longer occurring. Additionally, using an RNA folding algorithm, we predicted the secondary structures of the most potent aptamer sequence

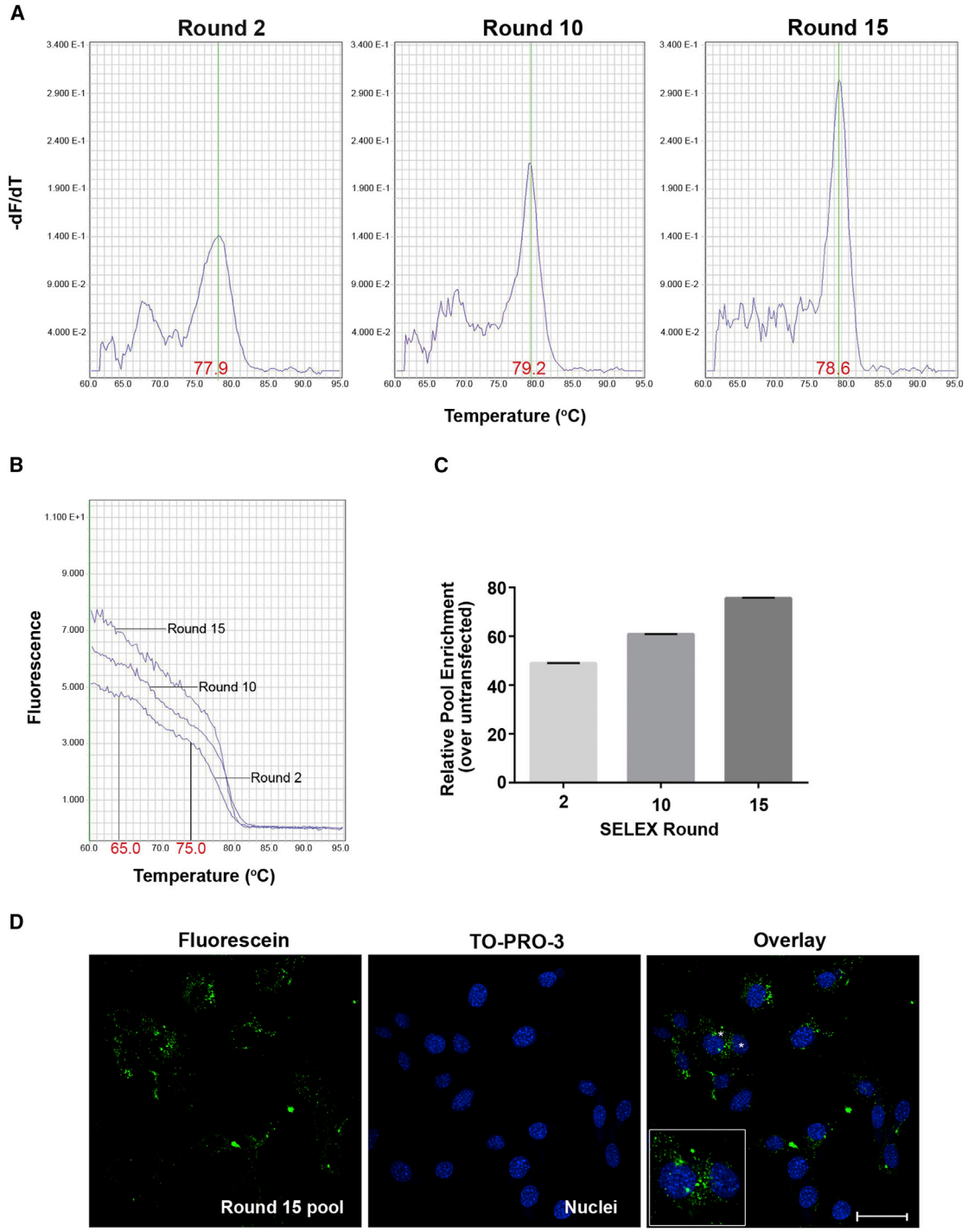

Figure 2. Assessment of the Selection Progression

(A) DNA melt assay profiles assessing the complexity of the RNA pools plotted as first negative derivative (−dF/dT) against temperature. From left to right: rounds 2, 10, and 15. (B) DNA melt assay profiles assessing the progress of the selection plotted as raw fluorescence against the temperature. (C) Quantification of aptamer enrichment during selection in the denoted rounds. Relative enrichment is shown as the fold-difference of aptamer pools over untransfected cells (mean ± SD). (D) Representative confocal microscopy images showing the internalization of the fluorescein-labeled RNA pool (green) at the final round (scale bar, 45.92 μm). Nuclei were stained blue. Magnified view is of area indicated by asterisks (*). See also Figure S2.

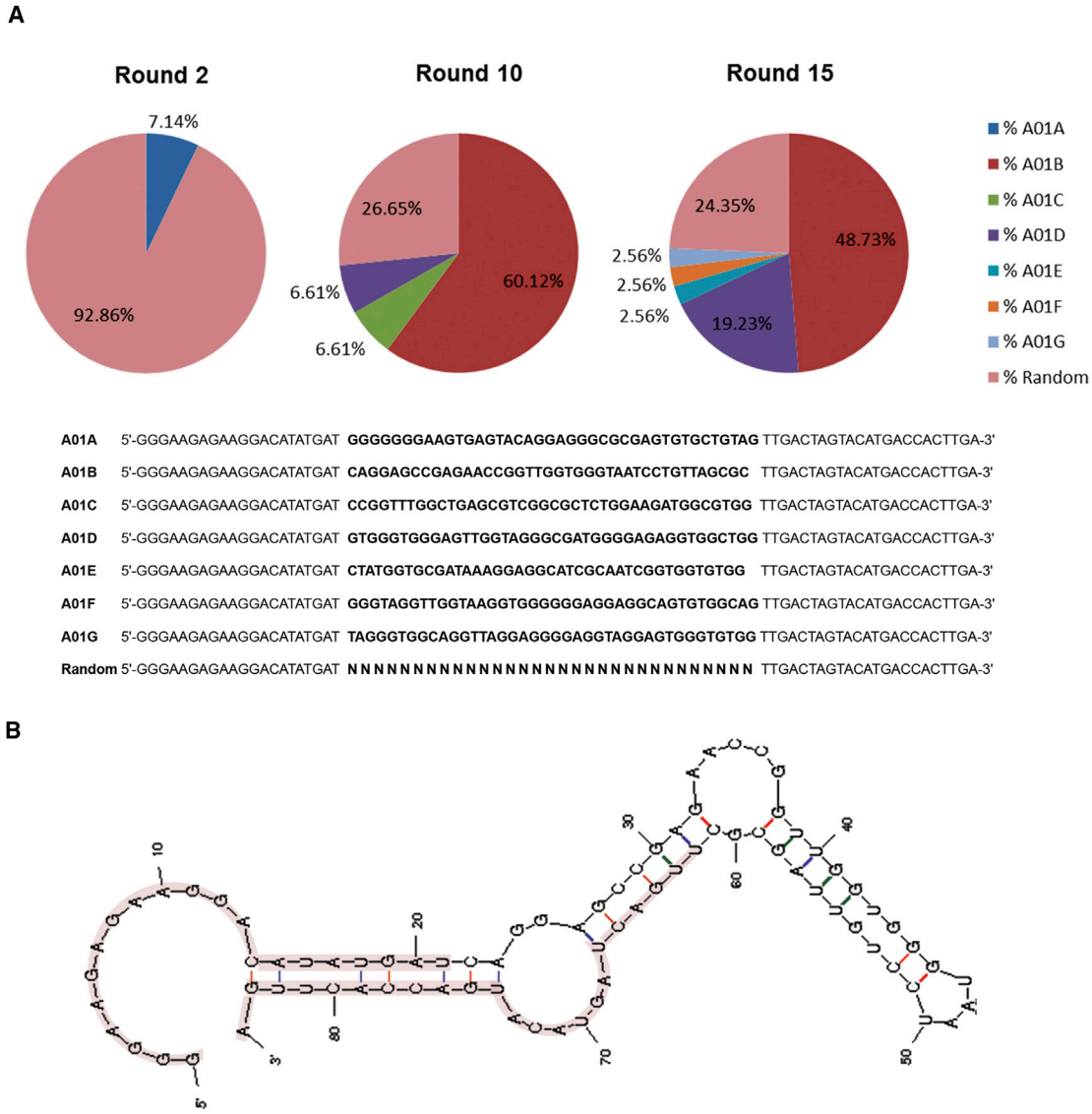

Figure 3. Convergence of Aptamer Sequences

(A) Multiple sequence alignment summary of the sequences recovered from the denoted rounds (top). Representative sequence for each identified aptamer, with the static (priming) regions shown in normal font and the variable region (N40) in boldface (bottom). (B) Secondary structure prediction of the dominant RNA aptamer (A01B). The static regions (nt 1–21 and 62–84) are highlighted. See also Figure S3.

(A01B). Among the four predicted structures, the structure with the lowest free energy, and thus most stable, is illustrated in Figure 3B. Together, these studies suggest that the A01B RNA sequence is a strong aptamer candidate for targeting skeletal muscle cells.

A01B RNA Aptamer Efficiently Enters Skeletal Muscle Cells in Culture

Due to its relative abundance in the selection rounds 10 and 15, A01B RNA aptamer was selected for further studies. First, the internalization and cellular localization of the selected aptamer was assessed in proliferating C2C12 muscle cell cultures (Figure 4A). The aptamer was conjugated to a cyanine dye (cyanine 3 [Cy3]) to enable detection by confocal microscopy. In addition, a scramble derivative of the aptamer (Cy3-conjugated scramble A01B) was used as a negative control to exclude non-specific aptamer binding. Cell membranes were stained with wheat germ agglutinin (WGA), Alexa Fluor 488 conjugate, thus enabling the identification of: (1) the cell membrane where the aptamer is expected to localize following target recognition, and (2) the internal endosomal membranes where the aptamer is expected to localize following internalization.[27] As illustrated, the internalization of the aptamer in C2C12 myoblasts was specific because minimal internalization was detected

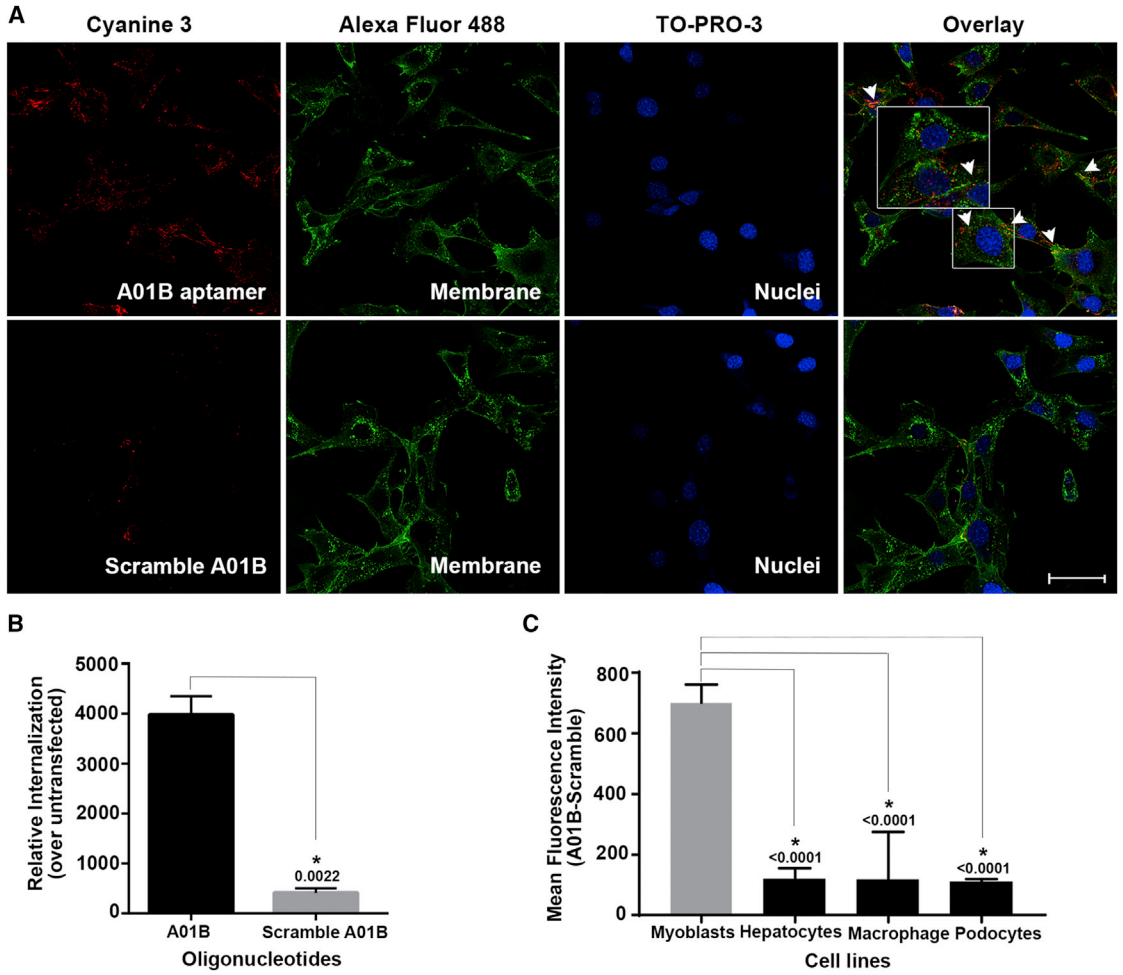

Figure 4. Internalization of A01B RNA Aptamer in Skeletal Muscle Cells

(A) Representative confocal images of C2C12 cells incubated with the A01B aptamer (red) or Scramble control (red). Cell membranes were stained green and nuclei blue (scale bar, 47.62 μm). White rectangles indicate regions of magnified view. Potential endosomal internalization (yellow) is indicated by arrowheads. (B) Quantification of internalized aptamer fraction in C2C12 cells. Internalization was expressed as fold-difference in expression relative to untreated samples (mean ± SD). *$p < 0.05$, Student's t test; n = 3. (C) Specificity of the A01B RNA aptamer for different cell lines. Mean fluorescence intensity (MFI) of A01B over Scramble was plotted for each cell line (mean ± SD). *$p < 0.05$, one-way ANOVA with Dunnett's multiple comparisons test; n = 3. See also Figure S4.

for the scramble A01B (Figure 4A). Additionally, the aptamer localized primarily in the cytoplasm of C2C12 myoblasts with minimal localization on the cell membrane of either of the cells or endosomal structures within the cytoplasm (arrowheads) (Figure 4A). In order to determine membrane-bound RNA aptamers, we also incubated cells with the aptamer at 4°C (Figure S4A). Confocal microscopy showed that a significant amount of the aptamer was bound on the membrane as a result of the cold incubation. Following removal of the non-specific sequences, additional incubation was performed at 37°C to facilitate internalization of the membrane-bound aptamers. Fluorescence was also present following incubation at 37°C, suggesting that the detected signal corresponds to specifically (and rapidly) internalizing RNA aptamers (Figure S4A, row 3). Additionally, the decrease in the fluorescent signal of the scramble A01B, from 4°C to 37°C, indicates that it is a suitable negative control for assessing aptamer internalization (Figure S4A, rows 2 and 4).

Consequently, the specific internalized fraction of the aptamer was next quantitated using qPCR (Figure 4B). For this assay, equal amounts of unlabeled aptamer and scramble aptamer were incubated with the target cells. Consistent with the previous data, the scramble aptamer showed very low internalization efficiency in target cells. On the contrary, the aptamer demonstrated a statistically significant ($p < 0.05$) internalization ability when compared with the scramble control, suggesting aptamer specificity. Moreover, the use of unlabeled aptamer and scramble control maintained the favorable difference that was previously observed between the two by confocal microscopy, showing that the presence of a label does not compromise the efficiency of the aptamer (Figures 4A and 4B). One of the

aims of this work was to select and develop aptamers with target specificity to skeletal muscle. During *in vivo* experimentation, aptamers may be faced with several possible routes which will result in absorption by other tissue.[12,28,29] It is well established that oligonucleotides may be well absorbed by the liver and the kidney following systemic delivery.[13] As a next experiment and in order to determine whether the evolved A01B RNA aptamer enters preferentially in skeletal muscle cells, the affinity of the aptamer for myoblasts relative to other cell lines was assessed by flow cytometry (Figure 4C). Myoblasts showed higher absolute incorporation of the aptamer compared with hepatocytes and podocytes, measured as absolute fluorescence intensity (AFI) of Cy3 conjugate aptamer and scramble control (Figure S4B). Subtracting background incorporation of fluorescence for Scramble from that detected for A01B aptamer, myoblasts show greater background-corrected affinity for A01B than any of the other cell lines with extreme statistical significance (Figure 4C). Absolute differences for A01B therefore show a therapeutically relevant high-level enrichment of A01B in myoblasts compared with hepatocytes and podocytes (Figure 4C). These data support the data obtained via confocal microscopy and suggest that the A01B aptamer enters efficiently and specifically in skeletal muscle cells.

Although aptamers are known to be non-immunogenic, the necessity for their continuous or repeated administration for therapeutic application *in vivo* could potentially trigger non-specific immune activation.[30,31] Therefore, the potential capacity of the selected aptamer to activate the immune system was initially evaluated against immune cells *in vitro* (Figure 4C). We reasoned the use of monocytes and macrophages for this assessment because they are central cells of the innate immune system, responsible for defending against diverse pathogens, and thus could impact potential clinical use of the aptamer. Comparison of the absolute intensities of the two oligonucleotides showed that the macrophages/monocytes population had a generally high affinity for both of them (Figure S4B). However, similarly to hepatocytes and podocytes, subtracting the Scramble fluorescence from that detected for the aptamer, myoblasts show greater background-corrected affinity for A01B than macrophages/monocytes with extreme statistical significance (Figure 4C). These data suggest non-specific internalization via phagocytosis, although assessment of macrophages in their local environment is necessary to further validate this result.[32]

As previously illustrated in Figure 4A, a small fraction of the internalized aptamer localized in cytoplasmic structures proximal to the cell membranes, suggesting potential endosomal internalization. To further investigate this, we performed immunostaining with the early endosome marker EEA1 (early endosome antigen 1) following aptamer incubation (Figure 5A).[33–35] The selected aptamer showed little colocalization (yellow) with EEA1-stained endosomal structures as indicated by the white arrowheads in the overlay image. Moreover, endosomal internalization was further investigated by assessing as early as 30 min and up to 120 min with also minimal colocalization (arrowheads) observed at any magnification and time point tested (Figure 5B; Figure S5). Taken together, these results suggest that the aptamer escapes the endosome through a yet unknown mechanism, or that it internalizes also through a non-endosome-related pathway.

A01B RNA Aptamer Efficiently Enters Skeletal Muscle in Mice

Because the aptamer was selected against proliferating skeletal muscle cells, it was next necessary to test whether this aptamer could retain its recognition ability for myofibers as well. With the ultimate goal being the use of the selected aptamer as a delivery vehicle for the skeletal muscle, its localization within the tissue over that of the scramble A01B was first examined after local delivery (Figure 6A). At 30 min after injection, the A01B aptamer was present within myofibers of the tibialis anterior (TA) muscle. As opposed to mice injected with the A01B aptamer, the scramble control remained localized primarily in the region between myofibers (arrowheads) revealing no skeletal-muscle-specific binding (Figure 6A). These differences were also confirmed by RNA analysis, as seen in Figure 6B. Collectively, these results suggest that the A01B RNA aptamer enters myofibers efficiently *in vivo*, thus highlighting the potential to serve as a skeletal muscle delivery vehicle.

DISCUSSION

The present work describes the identification of the first skeletal muscle RNA aptamer that can potentially enhance the therapeutic outcome of current oligonucleotide gene therapies in muscular dystrophies. Importantly, we were able to identify an RNA aptamer that efficiently internalizes into proliferating skeletal muscle cells in culture. These characteristics were equally observed when the aptamer was administered intramuscularly, indicating a potential therapeutic application.

The recent advancements in the selection strategies (SELEX) from *in vitro* to *in vivo* have given the capability to generate aptamers that recognize diseased tissues and organs.[29,36,37] This was initially shown by Cheng et al.,[29] who successfully identified a brain-penetrating aptamer for targeting various payloads for the treatment of neurological disorders. In a similar manner, Mi et al.[36] were able to identify an RNA aptamer that localizes in a humanized mouse model of metastatic colorectal cancer. Despite the great potentials in identifying aptamers with clinical relevance, such an approach is not beneficial for the selection of skeletal muscle RNA aptamers.[36] Here, several different skeletal muscles have to be isolated throughout the body, which is technically challenging. On the other hand, the selection against only one skeletal muscle (e.g., TA muscle) as proof of concept adds bias to our aptamer selection and the therapeutic potentials of this approach. For these reasons, we chose to employ an *in vitro* cell-internalization SELEX strategy in cultured skeletal muscle cells. More specifically, the selection was performed against the murine C2C12 cell line, which is a well-established model of skeletal muscle development.[38] Because the goal was to identify aptamers that enhance specificity for the skeletal muscle, it would be more appropriate to use the differentiated C2C12 cells, because they resemble more closely the myofibers *in vivo*. Proliferating C2C12 cells were eventually selected as the target because of the widely known transfection difficulties of the former *in vitro*.[39,40]

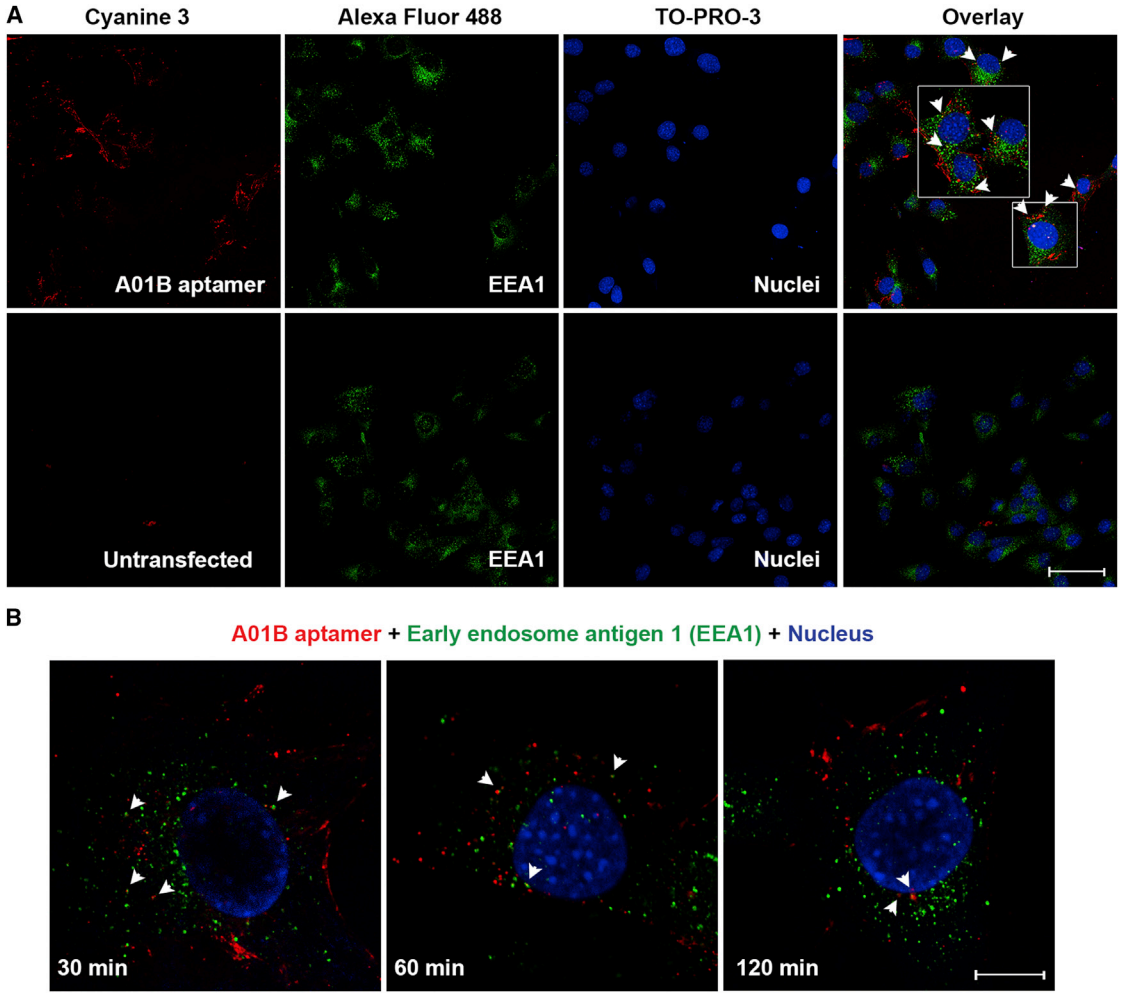

Figure 5. Assessment of Endosomal Internalization *In Vitro*

(A) Representative confocal images assessing endosomal internalization of the aptamer (red) at 120 min. The early endosome marker anti-EEA1 was stained green and the nuclei blue (scale bar, 56.2 μm). White rectangles indicate regions of magnified view. Colocalization is indicated by white arrowheads. (B) Representative confocal images assessing endosomal internalization of the aptamer (red) at various time points. The early endosome marker anti-EEA1 was stained green and the nuclei blue (scale bar, 99.3 μm). Colocalization is indicated by white arrowheads. See also Figure S5.

Another important consideration was the use of negative selection to exclude aptamer sequences that may be common between the target cells and other cell types. We initially reasoned the use of podocytes and hepatocytes because AONs tend to localize at high concentrations in kidney and liver, following systemic administration.[13,41,42] This indicates the need to select aptamers that remain in the circulation for longer. It was, however, unclear whether this approach would be advantageous for the identification of RNA aptamers with skeletal muscle specificity, or if it would make the evolution more challenging. For these reasons, no negative selection was performed, and both cell types were alternatively incorporated in the selection strategy. More specifically, when the most dominant sequence was identified, a comparison of its internalization efficacy among the target skeletal muscle cells and these cell types was performed. Our findings indicate that the internalization in both kidney and liver cells was non-specific (Figure 4C). One final consideration in our design was the length of the variable region. A shorter variable region can often be beneficial for selecting short aptamers to act as delivery vehicles but can also greatly limit the structural diversity. Alternatively, longer variable regions can provide the necessary structural diversity for the successful identification of aptamers.[43] In particular, a 40-nt variable region was used for the successful identification of several RNA aptamers *in vitro* and was therefore selected for our study as well.[44–47]

The selection strategy described herein resulted in the enrichment of RNA aptamers with efficient internalization in skeletal muscle cells (Figure 3). More specifically, one sequence (A01B RNA aptamer) was more frequent in both rounds (10 and 15) and was selected for further studies. This phenomenon of "one selection-one aptamer" is most likely the result of using the Sanger sequencing method where

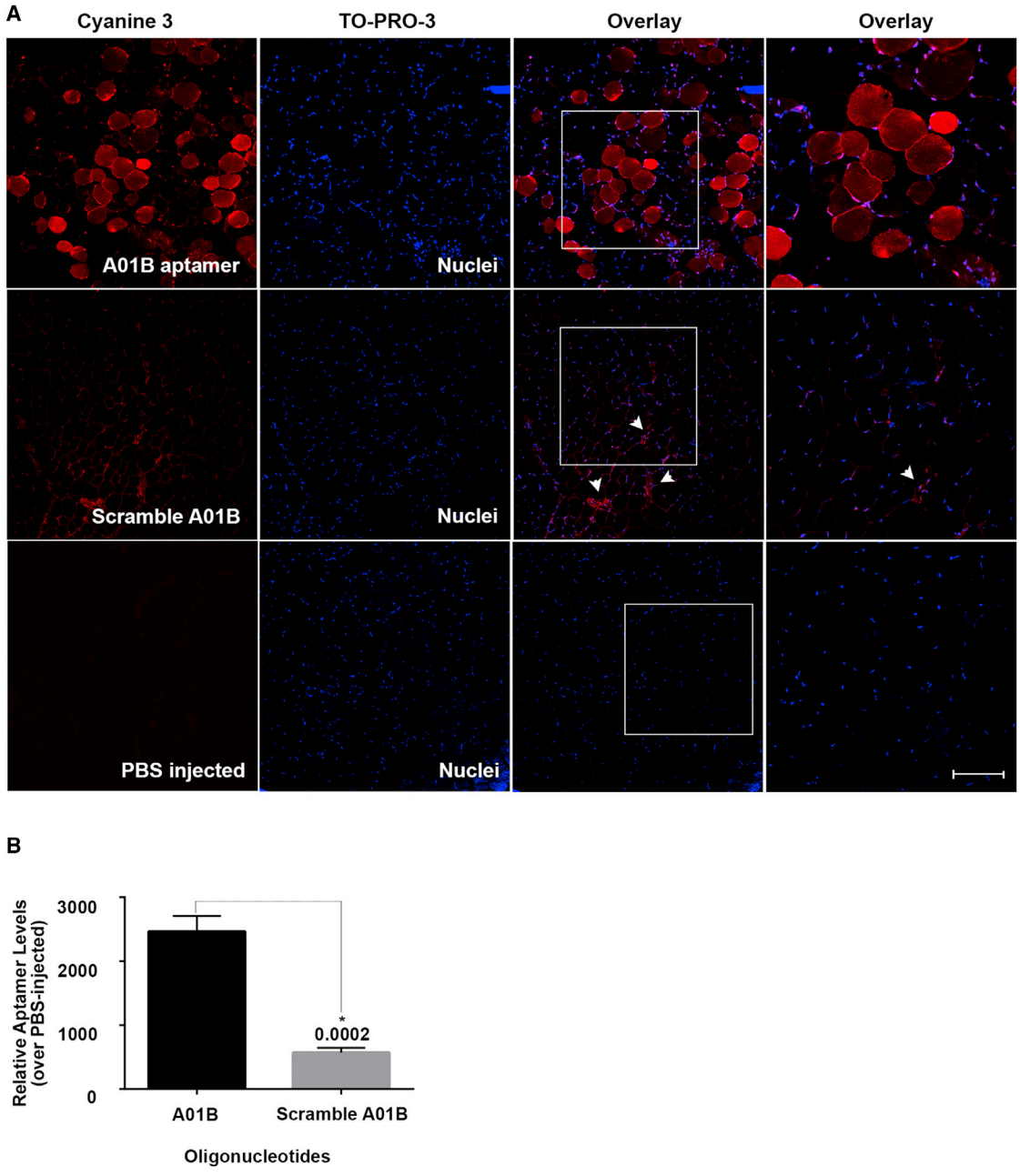

Figure 6. Internalization and Subcellular Localization of A01B RNA Aptamer *In Vivo*

(A) Representative confocal images of cross sections from the TA muscle of wild-type mice injected with A01B RNA aptamer (red), scramble A01B (red), or PBS (scale bar, 150 μm). Higher magnification imaging was captured for the areas indicated by white rectangles (scale bar, 75 μm). Nuclei were stained blue. Colocalization is indicated by white arrowheads. (B) Quantification of A01B RNA aptamer and scramble A01B levels in the skeletal muscle. Data were expressed as fold-difference in expression relative to PBS-injected samples (mean ± SD). *$p < 0.05$, Student's t test; $n = 3$.

only the most highly represented sequences are sequenced.[47–50] It is probable that more aptamer sequences with even higher binding affinities could have been identified with next-generation sequencing, as shown in more recent *in vitro* and *in vivo* SELEX works.[29,36,37,51,52] Nevertheless, we reasoned the use of a more conventional approach because this work is only the first step in the identification of RNA aptamers with skeletal muscle specificity. Additionally, because the ultimate goal is the targeted aptamer-mediated delivery of therapeutic oligonucleotides in muscular dystrophies, characterization of the aptamers' binding target was beyond the scope of this work. Therefore,

subsequent assessments were primarily focused on evaluating the cell internalization properties of the selected aptamer over the scramble control among a range of cell lines (skeletal muscle cells, hepatocytes, podocytes, macrophages, and monocytes). Our work *in vitro* shows that the A01B RNA aptamer enters efficiently and selectively into proliferating skeletal muscle cells (Figure 4). It is interesting, though, to note that when administered to the macrophages/monocytes population, both the aptamer and scramble control demonstrated an identically high cellular uptake (Figure S4B). This could relate to the small size of the aptamers and the general tendency of macrophages to phagocytose particles including oligonucleotides.[53]

Currently, several aptamer-drug complexes have exploited internalization; however, only a few studies further explored the mode of cellular delivery.[54] The findings of most of these examples suggest entry via receptor-mediated endocytosis and subsequent localization in endocytic vesicles such as endosomes.[26,27,55–58] Our confocal images utilizing an early endosome marker (EEA1) indicate minimal endosomal internalization (Figure 5). This small EEA1-positive aptamer fraction is probably targeted for degradation through maturation of early endosomes to late endosomes and subsequent fusion with lysosomes.[33,58] Recycling of this fraction back to the plasma membrane is highly unlikely because EEA1 has been shown to be a specific marker of the early sorting endosome with no association with the recycling endosome.[59] Consequently, these findings suggest that the aptamer is released to the cytoplasm probably through a mechanism of endosomal escape, as previously demonstrated by the Giangrande group.[60,61] In this study, a cellular toxin (saporin) with cytotoxic properties was conjugated to the A9g aptamer to assess its cytoplasmic delivery. Upon aptamer-mediated delivery of saporin to the cytoplasm, the toxin exerted its ribosome inactivating protein effects, thus leading to cell death.[34,35] Another possible explanation could be that the aptamer internalizes through more than one pathway where one of these is a non-endosome-related pathway, hence the red fluorescence (Figure 5). The latter is supported by the work of Van der Aa et al.,[62] who demonstrated interchangeable internalization of two well-established cationic polymers through two different endocytic routes (clathrin- and caveolae-dependent endocytosis). Whether internalization of the A01B aptamer is through any of the suggested mechanism (or other routes) requires further study.

Contrasting with more recent studies that question whether *in vitro*-generated aptamers can bind to their target *in vivo*, our aptamer remained functional when locally administered in mice.[29,36,37] As illustrated in Figure 6A, the aptamer exhibited a high fluorescent signal and internalization capacity within myofibers of the TA muscle. This could be attributed to the use of a Cell-SELEX protocol whose advantage, over the traditional selection against purified proteins, is the recognition of targets under their native conformation. This increases the likelihood to identify aptamers that are also functional *in vivo*.[63,64] The aforementioned result further suggested that the chemical substitution (from 2′-F- to 2′OMe-modified pyrimidines) did not alter the folding structures of the aptamer, which is also in agreement with the work of Cheng et al.[29] The 2′OMe chemistry was employed because it provides higher essential properties (nuclease resistance, stability) than 2′-F for *in vivo* applications.[65–67]

To date, the local delivery of therapeutic AONs in muscular dystrophies requires the use of electroporation to increase their uptake within the skeletal muscle.[68–73] For instance, in an animal model of DM1, pre-treatment with bovine hyaluronidase followed by intramuscular injection and electroporation of an all LNA (locked nucleic acid)-modified oligomer resulted in a significant reduction of nuclear retained RNA transcripts and correction of muscleblind like-protein (MBNL)-sensitive alternative splicing.[74] Despite the great effect in the distribution of oligonucleotides within the muscle, electroporation as a delivery method is not feasible for all affected muscles. Our *in vivo* findings suggest that the A01B RNA aptamer may potentially overcome this difficulty, a critical feature for entering the clinical settings. Another important feature for DM1 is their small size (3–5 nm) because it allows aptamers to pass freely across the nuclear membrane, through the nuclear pore complexes.[75,76] This could prove useful for the delivery of specific AONs against the nuclear retained toxic RNA. This toxic RNA ultimately results in the formation of ribonuclear foci, which is a key molecular hallmark of the disease.[77–79]

Systemic administration of RNA aptamers could also improve the therapeutic efficacy of AONs currently investigated in the treatment of DMD.[80] Recent studies show that the delivery efficiency of both the 2′-OMe PS AON and PMO is closely related to the "leaky" cell membrane, thus suggesting the passive diffusion as the mechanism of systemic delivery. This leads to a highly variable exon-skipping efficiency both between muscle and within the myofibers of individual muscles.[65,67,81] On the contrary, aptamer-mediated delivery of these oligonucleotides could significantly improve dystrophin expression and, most importantly, assist in maintaining adequate levels to almost all muscles including the heart, independently of membrane leakages.[80] Functional correction of the DMD phenotype with a high degree of dystrophin rescue in the heart was recently achieved in two mouse models with tricyclo-DNA, a new class of AONs.[41,82] Nevertheless, the tolerability (and therefore promise) of this chemistry by humans is still not known.[41] The use of an RNA aptamer to selectively deliver modified AONs to all muscles could also reduce the amount of the therapeutic dose and any dose-dependent toxic effects. Whether the conjugation of such AONs will render the aptamers' binding efficiency to target or vice versa is still unknown. Several chimeras with an aptamer and an siRNA part have been successfully synthesized by chemical synthesis of long oligonucleotides.[26,57] In other cases, joining of siRNAs to aptamers was achieved following their synthesis by covalent and non-covalent conjugation.[83]

Despite the great promise, further studies are needed to assess the aptamer's specificity for skeletal muscle and potential toxic effects following systemic administration. This will give the possibility to efficiently and safely target all muscles of the body. Truncation studies guided by RNA structure software packages will be needed to identify the smallest functional version of the aptamer that will allow conjugation of AONs of varying sizes without compromising tissue

penetration.[57,84] Nevertheless, the recent delivery of chemically modified messenger RNA therapeutics in gene therapy research[85,86] indicates that the current size of our aptamer may not necessarily be a limitation.[72,73] In addition, the therapeutic efficacy of aptamer-conjugated AONs will have to be assessed over the currently applied methodologies. This will be of critical importance to demonstrate the improved efficacy with aptamer delivery.

In summary, the cell-internalization SELEX protocol employed herein allowed the identification of the first RNA aptamer that enters efficiently in skeletal muscle. This aptamer could potentially serve as a muscle-specific delivery vehicle for a wide spectrum of therapeutic molecules, thus opening a new era of safe and targeted aptamer-mediated therapies for muscular dystrophies.

MATERIALS AND METHODS

Cell Culture and Mouse

The C2C12 mouse myoblast cell line (ECACC, Salisbury, UK) was maintained in DMEM supplemented with 10% fetal bovine serum (FBS), 2% L-glutamine (GlutaMAX), and 1% penicillin-streptomycin (PS) in a humidified incubator with 5% CO_2 at 37°C. For selection rounds, C2C12 cells were plated at a density of 7.3×10^6 per 100-mm Petri dish and 4×10^5 cells/well of a six-well plate for next day internalization assays. AML12 hepatocytes (ATCC, Middlesex, UK) were maintained in a 1:1 mixture of DMEM and Ham's F12 medium supplemented with 10% FBS, 1% Insulin-Transferrin-Selenium (ITS-G) (100×), 1% PS, and 40 ng/mL dexamethasone (Sigma-Aldrich) in a humidified chamber with 5% CO_2 and 37°C. For next day internalization assays, cells were plated at a density of 9×10^5 cells/well of a six-well plate. AB8/13 podocytes (glomerular epithelial cells) were obtained from Prof. Saleem at the University of Bristol (Bristol, UK). Cells were maintained in RPMI 1640 medium (GlutaMAX Supplement) supplemented with 10% FBS, 1% ITS-G, and 1% PS. For proliferation, podocytes were maintained in a humidified chamber with 5% CO_2 at 33°C. For differentiation, cells were plated at 3×10^5 cells/well of a six-well plate and maintained at 33°C. At 50%–60% confluency, cells were transferred from 33°C to a 37°C and 5% CO_2 humidified chamber for 14 days, with daily medium renewal. The J774A.1 macrophages/monocytes cell line (ATCC, Middlesex, UK) was maintained in DMEM supplemented with 10% FBS, 2% L-glutamine, and 1% PS in a humidified chamber with 5% CO_2 at 37°C. For next day internalization assays, cells were plated at a density of 1×10^6 cells/well of a six-well plate. All media and supplements were purchased from GIBCO by Thermo Fisher Scientific (Waltham, MA, USA). C57BL/6 mice were purchased from Jackson Laboratory (Bar Harbor, MI, USA). All animal studies were approved by the local committee for animal experimentation. All experiments were performed at 8 weeks of age.

Aptamer and Control Sequences

For confocal imaging, the aptamer and control sequences were synthesized by TriLink BioTechnologies (San Diego, CA, USA). Oligonucleotides were received as lyophilized powder and resuspended in Tris-EDTA (TE) buffer (pH 8; Ambion, Austin, TX, USA) at a final concentration of 100 μM. Next, they were folded in folding buffer (1 mM $MgCl_2$, 1× DPBS [pH 7.5]) to obtain their secondary structures. Folding conditions were 10 min at 70°C, snap-cooled on ice for 5 min, and slowly cooled to 37°C for 30 min. Oligonucleotides were ordered with the following modifications: 5′-Cy3 fluorescent dye, internal 2′-fluorine or 2′-O-methyl pyrimidines (C, U), and a phosphodiester backbone.

Preparation of the RNA Library

The initial single-stranded DNA library (sequence adapted from previous work;[87] Table S1) contained 40 nt of random sequence at an equimolar concentration and was synthesized by Eurofins Genomics (Wolverhampton, UK). The random region was flanked by constant regions, which served as the primer binding sites during PCR amplification. The DNA library was amplified by PCR in the presence of Taq DNA polymerase (QIAGEN, Manchester, UK) and 1 μM (final concentration) T7P Forward and Reverse primers also purchased by Eurofins Genomics (Table S1) The PCR amplification protocol was: 94°C for 5 min, followed by 1 cycle of heating at 94°C for 30 s, 53°C for 30 s, and 72°C for 1 min, followed by 12–18 cycles of heating at 94°C for 30 s, 59°C for 30 s, and 72°C for 1 min. A final extension step was performed for 5 min at 72°C. The forward primer included the minimum T7 promoter sequence for *in vitro* transcription (Table S1). The expected 107-bp product size was confirmed on an 8% native PAGE gel. Next, the PCR product was *in vitro* transcribed for 16 hr at 37°C using the Durascribe T7 transcription kit (Epicenter, Madison, WI, USA) where 2′-F pyrimidines were incorporated to produce nuclease-resistant RNA transcripts. The expected 84-nt RNA library was confirmed on a 12% denaturing (7 M urea) PAGE gel; then the remaining RNA was purified by phenol-chloroform extraction (acid-phenol:chloroform was purchased from Ambion) followed by ethanol precipitation as previously described.[88] The purified RNA library was quantified with a NanoDrop ND-1000 Spectrophotometer at A260.

In Vitro Selection of RNA Aptamers for C2C12 Myoblasts

C2C12 myoblasts were cultured in Petri dishes as described under cell culture methods. The cell-internalization SELEX procedure was performed as previously described.[51] In brief, for each round of selection, 1500 pmol RNA was folded in 1 mL of Opti-MEM (GIBCO) as previously described for A01B RNA aptamer and scramble A01B control sequence. C2C12 myoblasts were washed 1× with 5 mL of warm DPBS (GIBCO), 3× with 5 mL of Opti-MEM, and incubated with 5 mL of Opti-MEM supplemented with 100 μg/mL yeast tRNA (Invitrogen, Carlsbad, CA) for 15 min at 37°C, to block non-specific binding. Next, the blocking medium was discarded and the folded RNA library was added in 9 mL of fresh Opti-MEM for 120 min for the first six rounds with frequent agitation. For rounds 7–9 and 10–12, the library was added for 90 and 60 min, respectively. For rounds 13 and 14, the incubations time was further decreased to 30 min, whereas for the final round (round 15), the library was incubated for 15 min.

Following incubation of the RNA library, C2C12 cells were washed three times with ice-cold DPBS to remove unbound sequences.

Membrane-bound sequences were removed with salt washes utilizing a brief ice-cold salt wash (+0.5 M NaCl in DPBS) followed by a second salt wash for 5 min at 4°C. Excess salt wash was removed with a final wash with ice-cold DPBS. To further increase the stringency conditions, we increased the number and time of washes during *in vitro* selection as described in Table 1. Next, cells were dissociated with 0.25% Trypsin-EDTA (GIBCO) for 1 min at 37°C. Trypsin was inactivated with the addition of 9 mL of growth medium. Cells were then centrifuged at 300 *g* for 5 min in a cold centrifuge and gently resuspended in 1 mL of DPBS. Cells were pelleted again as described above, resuspended in 100 µL of DPBS, and treated with 5 µL of Riboshredder RNase cocktail (Epicenter, Madison, WI, USA) for 15 min at room temperature. This step ensures digestion of remaining surface-bound aptamers.[89] The volume was increased to 1 mL, and the cells were washed thrice in ice-cold DPBS as described above. The pelleted RNA was stored at −80°C. The internalizing RNAs were recovered as described later in the RNA Extraction section.

Purified RNA was next quantified by NanoDrop ND-1000 Spectrophotometer at A260, and 0.5–2 µg was reverse transcribed in cDNA using the M-MuLV Reverse Transcriptase (200 U/µL; NEB, Ipswich, MA, USA) in the presence of 250 µM dinucleotide triphosphate (dNTP) (Sigma-Aldrich) and 3 µM (final concentration) reverse primer (Table S1) in a 40-µL reaction. 1–5 µg of cDNA was then PCR amplified (100-µL reaction volume) and *in vitro* transcribed to produce the RNA pool for the next selection round as described earlier in the Preparation of the RNA Library section.

Sequencing

RNA pools from rounds 2, 10, and 15 were reverse transcribed and PCR amplified as described earlier. Next, 1 µL from each PCR product was cloned into the TOPO TA cloning vector pCR 2.1 (Invitrogen) and transformed into *Escherichia coli* DH5α competent cells, and individual colonies from Luria-Bertani plates containing isopropyl β-D-1-thiogalactopyranoside (IPTG)/X-gal were selected. 100 clones were selected from each selection round. Each clone was purified using the QuickLyse Miniprep Kit (QIAGEN) and prepared for sequencing using the BigDye Terminator v1.1 Cycle Sequencing Kit (Life Technologies, Carlsbad, CA, USA) as per the manufacturer's instructions. 29 cycles of cycle sequencing were performed to amplify the selected fragments using sequencing primers (M13 Forward −20 and M13 Reverse) (Table S1) supplied with the cloning kit. The samples were then purified with Performa DTR Gel Filtration Cartridges (Edge Bio, Gaithersburg, MD, USA) and loaded on an ABI 3130xl Genetic Analyzer (Applied Biosystems by Thermo Fisher Scientific, Carlsbad, CA, USA). Using the ABI 31xl software, we produced base-call files and quality scoring was run. Sequencing analysis was performed using the KB Basecaller 1.4 internal software. The raw sequencing data were further analyzed using the Applied Biosystems SeqScape Software v2.5. Any sequences that were incomplete or incorrect were filtered out. Next, Clustal Omega, an online multiple sequence alignment tool (https://www.ebi.ac.uk/Tools/msa/clustalo/), was used to align and cluster all unique sequences into groups of the same sequence.

RNA Secondary Structure Prediction

The mfold web server (http://unafold.rna.albany.edu/?q=mfold/RNA-Folding-Form) was used to predict the secondary structures of the most prominent sequence(s) following sequencing. Each sequence was added in FASTA format as linear RNA molecules. The structure predictions were made using default settings.

qRT-PCR

To assess the selection progress, we incubated 100 pmol RNA pools from selection rounds 2, 10, and 15 with C2C12 cells for 90 min. To assess internalization of the aptamer, we incubated 100 pmol of the A01B aptamer, scramble A01B control sequence for 120 min with the target cell line (C2C12 myoblasts). Cells were then washed 1× with 1 mL of ice-cold DPBS, 1× with 1 mL of ice-cold salt wash, and subsequently incubated with 1 mL of salt wash for 5 min at 4°C. Cells were washed a final time with 1 mL of ice-cold PBS and resuspended in 100 µL of PBS. Membrane-bound aptamers were digested with 5 µL of Riboshredder as previously described. Cellular RNA was extracted using TRIzol reagent (Life Technologies) as described in the RNA Extraction section.

To confirm the specificity of the selected aptamer for the skeletal muscle, 1 nmol Cy3-conjugated A01B aptamer or Cy3-conjugated scramble A01B control (both with 2′-OMe chemically modified pyrimidines) was folded in 30 µL of folding buffer (1 mM $MgCl_2$ in 1× DPBS). The oligonucleotides were then injected locally in the TA muscle of three C57BL/6 mice (8 weeks old), under general anesthesia (intraperitoneal injection of 2,2,2-tribromoethanol, 250 mg/kg; Sigma-Aldrich). The mice were sacrificed by cervical dislocation at 30 min after injection, and the TA muscles were isolated for RNA extraction with TRIzol reagent (Life Technologies) followed by phenol-chloroform purification and ethanol precipitation.[88] Mice injected with 30 µL of PBS were used as controls.

The amount of RNA (either from cells or tissue) was quantitated using a NanoDrop ND-1000 spectrophotometer, and 500 ng of DNase I-treated RNA was input for reverse transcription using M-MuLV Reverse Transcriptase (NEB) and a random hexamer primer (3 µM, final concentration) (Eurofins Genomics). Relative abundance of RNA species (RNA libraries or individual aptamer sequence) was quantitated using qRT-PCR with SELEX-specific primers (0.4 µM, final concentration) (Table S1) and Applied Biosystems Power SYBR Green PCR Master Mix (Thermo Fisher Scientific, Carlsbad, CA). Real-time PCR was performed in triplicate on each cDNA sample using the Applied Biosystems Sequence Detection System 7900HT Fast Real-Time PCR System and a standard PCR protocol for SYBR green reactions followed by melt curve analysis. Data were analyzed with the $\Delta\Delta C_T$ method of quantification (also referred to as comparative C_T method), whereby C_T values for the target (SELEX primers) were normalized to the levels of the housekeeping gene *glyceraldehyde-3-phosphate dehydrogenase* (*GAPDH* F and R; Eurofins Genomics) (Table S1). Relative quantity (RQ) values were then expressed as fold-difference in expression over untreated or PBS-injected samples as per the mathematical formula.[90]

DNA Melt Curve Analysis

Dissociation curves were carried out at the end of each qRT-PCR experiment. All components were first denatured at 95°C, followed by complete annealing at 60°C and then by a gradual increase in temperature up to 95°C. Fluorescence intensity was monitored during this final temperature increase, resulting in the generation of dissociation curves. The raw DNA melt assay data were plotted as fluorescence intensity (F) or first negative derivative (−dF/dT) versus temperature (°C).

Confocal Microscopy

To assess the selection progress, we generated fluorescent RNA pools using the Silencer siRNA Labeling Kit with FAM dye (Ambion) as per the manufacturer's instructions. To assess the cellular internalization of A01B aptamer in C2C12 myoblasts, we purchased Cy3-conjugated A01B aptamer and Cy3-conjugated scramble A01B control (both with 2′-F chemically modified pyrimidines) from TriLink BioTechnologies as previously described. In both cases, C2C12 myoblasts were seeded on sterile cover glasses (Heinz Herenz, Hamburg, Germany) placed in six-well plates. At 90% confluency, cells were washed 1× with 1 mL of DPBS, 3× with 1 mL of Opti-MEM, and incubated with 100 μg/mL yeast tRNA for 15 min at 37°C. Next, the medium was discarded and 100 pmol of either fluorescein-labeled RNA pools, Cy3-conjugated A01B aptamer, or Cy3-conjugated scramble A01B were incubated with the cells at 37°C in 1 mL of Opti-MEM supplemented with 100 μg/mL yeast tRNA (Invitrogen). Cells were incubated with the oligonucleotides for 90–120 min with frequent agitation (every 15 min). C2C12 cells were next washed 1× with 1 mL of ice-cold DPBS, 1× with 1 mL of ice-cold salt wash, and subsequently incubated with 1 mL of salt wash for 5 min at 4°C. One final wash with 1 mL of ice-cold DPBS was performed followed by fixation with 2% paraformaldehyde for 5 min and then 4% paraformaldehyde for an additional 5 min at 4°C. TO-PRO-3 nuclear stain (T3605; Thermo Fisher Scientific) was next applied for 15 min at room temperature at a dilution of 1:1,000 in PBS. Coverslips were washed 2× for 5 min with 1 mL of PBS and mounted with Dako fluorescent mounting medium onto Poly-Prep slides (Sigma-Aldrich). Slides were left to dry for 30 min at room temperature in the dark and then stored at 4°C overnight. Images were taken on a Leica TCS SP5 confocal microscope. For individual aptamer assays, cell membranes were also stained for 10 min at room temperature with wheat germ agglutinin, Alexa Fluor 488 conjugate (W11261; Thermo Fisher Scientific) at a final concentration of 10 μg/mL.

To evaluate the subcellular localization of the aptamer within the skeletal muscle, we prepared a 10-μm thin section from Cy3-conjugated A01B aptamer, Cy3-conjugated scramble A01B (both chemically modified with 2′-OMe pyrimidines), or PBS-injected mice using a cryostat. Sections representative of the entire TA muscle were collected on glass slides (Superfrost Plus; VWR, Atlanta, GA, USA) as described previously.[91] Next, the slides were fixed with 4% ice-cold paraformaldehyde for 10 min at room temperature and stained with TO-PRO-3 nuclear stain as described previously. Samples were mounted with an antifade fluorescence mounting medium (Dako, Santa Clara, CA, USA) and allowed to dry for 30 min at room temperature. Images were obtained with a Leica TCS SP5 confocal microscope as described previously.

Immunocytochemistry

To assess endosomal internalization, we incubated 100 pmol Cy3-conjugated A01B aptamer with C2C12 myoblasts for 30–120 min at 37°C as described earlier under the section Confocal Microscopy. Following fixation, cells were processed for immunocytochemical analysis of the EEA1 early endosomal marker. To remove excess fixative, we washed cells twice for 5 min with 1 mL of ice-cold PBS and then permeabilized them with 3 mL of ice-cold 100% methanol for 3 min in the freezer. Cells were then washed 3× with 1 mL of PBS supplemented with Tween 20 (Scharlau, Barcelona, Spain) at a final concentration of 0.1% (PBS-T). Blocking of non-specific binding was performed with 5% normal goat serum (Biosera, Nuaillé, France) in PBS-T for 60 min at room temperature. Coverslips were transferred in a humidity chamber; then the primary antibody rabbit EEA1 (C45B10) (Cell Signaling Technologies, Danvers, MA, USA) was applied at 1:100 in blocking buffer and incubated overnight at 4°C. The next day, coverslips were washed 3× with 1 mL of PBS-T and then incubated with Invitrogen Alexa Fluor Plus 488 goat anti-rabbit IgG secondary antibody at a dilution of 1:500 in blocking buffer for 60 min at room temperature. Coverslips were washed 3× 5 min with 1 mL of PBS-T; then TO-PRO-3 nuclear stain was applied for 15 min at room temperature at a dilution of 1:1,000 in PBS. Coverslips were washed 2× with 1 mL of PBS and mounted with Dako fluorescent mounting medium onto Poly-Prep slides. Slides were left to dry for 30–60 min at room temperature. Images were taken on a Leica TCS SP5 confocal microscope. Single-cell magnifications were achieved by applying the 60× oil objective followed by additional electronic magnification.

Flow Cytometry

The affinity of the aptamer for myoblasts relative to other cell lines was assessed by flow cytometry in three independent experiments for each cell type. In brief, 100 pmol Cy3 conjugate A01B RNA aptamer or scramble A01B was incubated with C2C12 myoblasts, AML12 hepatocytes, AB8/13 podocytes, and J774A.1 macrophages/monocytes for 60 min at 37°C as described under the section qRT-PCR. Cy3 (for the aptamer and scramble control), SYTOX Red (for live/dead discrimination) (S34859; Thermo Fisher Scientific) fluorescence, and background fluorescence were determined with Cyflow Cube 8 (Sysmex Partec, Görlitz, Germany). Further analysis was performed using FCS Express 4 Flow cytometry software. Representative fluorescence intensity histograms were plotted for each experiment using also FCS Express 4 Flow cytometry software. AFI of each oligonucleotide per cell type or mean fluorescence intensity (MFI ± SD) of A01B for each cell type was plotted. For AFI, the mean from three independent experiments ± SD was plotted. MFI was calculated by subtracting the background-corrected fluorescence intensity for Scramble from the background-corrected fluorescence intensity of the A01B (A01B-Scramble A01B).

RNA Extraction

Total RNA from treated and untreated C2C12 cell pellets was extracted with 500 μL of TRIzol reagent (Life Technologies) as per the manufacturer's instructions. To obtain pure cellular RNA, we resuspended pellets in 200 μL of RNase-free water followed by phenol-chloroform purification and ethanol precipitation as previously described.[88] For total RNA extraction, oligonucleotide or PBS-injected TA muscles were snap-frozen in liquid-nitrogen-cooled isopentane (Thermo Fisher Scientific) to quench RNA degradation. Following overnight incubation at −80°C, muscles were homogenized with 1 mL of TRIzol using the Precellys 24 homogenizer and lysing kit (Bertin Instruments, Italy).

Subsequently, all RNA samples were treated with DNase I (RNase-free) from New England BioLabs or with Ambion DNA-free DNase Treatment and Removal Reagents as per the manufacturer's instructions. Concentration and purity of total RNA were determined using the NanoDrop ND-1000 spectrophotometer at A260 before storage at −80°C.

Statistical Analysis

For each analysis, three independent experiments were performed. Mean and SDs were then determined using Microsoft Excel 2013 and/or GraphPad Prism 7. All data were plotted using GraphPad Prism 7. For pairwise comparisons, statistical difference between the denoted means was investigated using Student's t test. For comparisons of more than two treatment groups, statistical difference between the denoted means was investigated by one-way ANOVA with Dunnett's multiple comparisons test. Significance was set up at a p value of 0.05 for all experiments.

Accession Number

The accession number for the A01B RNA sequence has been deposited to the DNA Data Bank of Japan (DDBJ): LC340032.

SUPPLEMENTAL INFORMATION

Supplemental Information includes five figures and one table and can be found with this article online at https://doi.org/10.1016/j.omtn.2017.12.004.

AUTHOR CONTRIBUTIONS

Conceptualization, L.A.P.; Methodology, S.P.; Validation, S.P. and C.W.L.; Formal Analysis, S.P. and C.W.L.; Investigation, S.P., N.M., and C.W.L.; Resources, L.A.P.; Data Curation, S.P. and C.W.L.; Writing – Original Draft, S.P.; Writing – Review & Editing, L.A.P., N.P.M., M.K., and S.P.; Visualization, S.P.; Supervision, L.A.P. and N.P.M.; Funding Acquisition, L.A.P.

CONFLICTS OF INTEREST

The authors declare no conflicts of interest.

ACKNOWLEDGMENTS

We thank Dr. Antonis Antoniou for technical assistance in setting up the SeqScape software (resequencing package) to the project's needs and Dr. Christiana Demetriou for assistance in statistical analysis. We would also like to thank the University of Bristol, especially Dr. Moin A. Saleem and Lan Ni, for providing the AB8/13 podocytes. This work was supported by grants to L.A.P. from TELETHON Cyprus (33173117) and the A.G. Leventis Foundation (Leventis Foundation).

REFERENCES

1. Flanigan, K.M. (2012). The muscular dystrophies. Semin. Neurol. *32*, 255–263.
2. Chamberlain, J.S. (2002). Gene therapy of muscular dystrophy. Hum. Mol. Genet. *11*, 2355–2362.
3. Aartsma-Rus, A., and van Ommen, G.J. (2007). Antisense-mediated exon skipping: a versatile tool with therapeutic and research applications. RNA *13*, 1609–1624.
4. van Deutekom, J.C., Janson, A.A., Ginjaar, I.B., Frankhuizen, W.S., Aartsma-Rus, A., Bremmer-Bout, M., den Dunnen, J.T., Koop, K., van der Kooi, A.J., Goemans, N.M., et al. (2007). Local dystrophin restoration with antisense oligonucleotide PRO051. N. Engl. J. Med. *357*, 2677–2686.
5. Kinali, M., Arechavala-Gomeza, V., Feng, L., Cirak, S., Hunt, D., Adkin, C., Guglieri, M., Ashton, E., Abbs, S., Nihoyannopoulos, P., et al. (2009). Local restoration of dystrophin expression with the morpholino oligomer AVI-4658 in Duchenne muscular dystrophy: a single-blind, placebo-controlled, dose-escalation, proof-of-concept study. Lancet Neurol. *8*, 918–928.
6. Cirak, S., Arechavala-Gomeza, V., Guglieri, M., Feng, L., Torelli, S., Anthony, K., Abbs, S., Garralda, M.E., Bourke, J., Wells, D.J., et al. (2011). Exon skipping and dystrophin restoration in patients with Duchenne muscular dystrophy after systemic phosphorodiamidate morpholino oligomer treatment: an open-label, phase 2, dose-escalation study. Lancet *378*, 595–605.
7. Goemans, N.M., Tulinius, M., van den Akker, J.T., Burm, B.E., Ekhart, P.F., Heuvelmans, N., Holling, T., Janson, A.A., Platenburg, G.J., Sipkens, J.A., et al. (2011). Systemic administration of PRO051 in Duchenne's muscular dystrophy. N. Engl. J. Med. *364*, 1513–1522.
8. Aartsma-Rus, A., and Krieg, A.M. (2017). FDA approves Eteplirsen for Duchenne muscular dystrophy: the next chapter in the Eteplirsen saga. Nucleic Acid Ther. *27*, 1–3.
9. Nakamori, M., Gourdon, G., and Thornton, C.A. (2011). Stabilization of expanded (CTG)●(CAG) repeats by antisense oligonucleotides. Mol. Ther. *19*, 2222–2227.
10. Wheeler, T.M., Leger, A.J., Pandey, S.K., MacLeod, A.R., Nakamori, M., Cheng, S.H., Wentworth, B.M., Bennett, C.F., and Thornton, C.A. (2012). Targeting nuclear RNA for in vivo correction of myotonic dystrophy. Nature *488*, 111–115.
11. Wheeler, T.M., Sobczak, K., Lueck, J.D., Osborne, R.J., Lin, X., Dirksen, R.T., and Thornton, C.A. (2009). Reversal of RNA dominance by displacement of protein sequestered on triplet repeat RNA. Science *325*, 336–339.
12. Juliano, R.L. (2016). The delivery of therapeutic oligonucleotides. Nucleic Acids Res. *44*, 6518–6548.
13. Geary, R.S., Norris, D., Yu, R., and Bennett, C.F. (2015). Pharmacokinetics, biodistribution and cell uptake of antisense oligonucleotides. Adv. Drug Deliv. Rev. *87*, 46–51.
14. Brolin, C., and Shiraishi, T. (2011). Antisense mediated exon skipping therapy for duchenne muscular dystrophy (DMD). Artif. DNA PNA XNA *2*, 6–15.
15. Goyenvalle, A., Seto, J.T., Davies, K.E., and Chamberlain, J. (2011). Therapeutic approaches to muscular dystrophy. Hum. Mol. Genet. *20* (R1), R69–R78.
16. Hasegawa, H., Savory, N., Abe, K., and Ikebukuro, K. (2016). Methods for improving aptamer binding affinity. Molecules *21*, 421.
17. White, R.R., Sullenger, B.A., and Rusconi, C.P. (2000). Developing aptamers into therapeutics. J. Clin. Invest. *106*, 929–934.
18. Germer, K., Leonard, M., and Zhang, X. (2013). RNA aptamers and their therapeutic and diagnostic applications. Int. J. Biochem. Mol. Biol. *4*, 27–40.
19. Yan, A.C., and Levy, M. (2009). Aptamers and aptamer targeted delivery. RNA Biol. *6*, 316–320.

20. Guo, P. (2010). The emerging field of RNA nanotechnology. Nat. Nanotechnol. *5*, 833–842.

21. Zhou, J., Bobbin, M.L., Burnett, J.C., and Rossi, J.J. (2012). Current progress of RNA aptamer-based therapeutics. Front. Genet. *3*, 234.

22. Ellington, A.D., and Szostak, J.W. (1990). In vitro selection of RNA molecules that bind specific ligands. Nature *346*, 818–822.

23. Chu, T.C., Twu, K.Y., Ellington, A.D., and Levy, M. (2006). Aptamer mediated siRNA delivery. Nucleic Acids Res. *34*, e73.

24. Zhou, J., and Rossi, J.J. (2011). Cell-specific aptamer-mediated targeted drug delivery. Oligonucleotides *21*, 1–10.

25. Kruspe, S., Mittelberger, F., Szameit, K., and Hahn, U. (2014). Aptamers as drug delivery vehicles. ChemMedChem *9*, 1998–2011.

26. McNamara, J.O., 2nd, Andrechek, E.R., Wang, Y., Viles, K.D., Rempel, R.E., Gilboa, E., Sullenger, B.A., and Giangrande, P.H. (2006). Cell type-specific delivery of siRNAs with aptamer-siRNA chimeras. Nat. Biotechnol. *24*, 1005–1015.

27. Benedetto, G., Hamp, T.J., Wesselman, P.J., and Richardson, C. (2015). Identification of epithelial ovarian tumor-specific aptamers. Nucleic Acid Ther. *25*, 162–172.

28. Healy, J.M., Lewis, S.D., Kurz, M., Boomer, R.M., Thompson, K.M., Wilson, C., and McCauley, T.G. (2004). Pharmacokinetics and biodistribution of novel aptamer compositions. Pharm. Res. *21*, 2234–2246.

29. Cheng, C., Chen, Y.H., Lennox, K.A., Behlke, M.A., and Davidson, B.L. (2013). In vivo SELEX for identification of brain-penetrating aptamers. Mol. Ther. Nucleic Acids *2*, e67.

30. Avci-Adali, M., Steinle, H., Michel, T., Schlensak, C., and Wendel, H.P. (2013). Potential capacity of aptamers to trigger immune activation in human blood. PLoS ONE *8*, e68810.

31. Kong, H.Y., and Byun, J. (2013). Nucleic acid aptamers: new methods for selection, stabilization, and application in biomedical science. Biomol. Ther. (Seoul) *21*, 423–434.

32. Gustafson, H.H., Holt-Casper, D., Grainger, D.W., and Ghandehari, H. (2015). Nanoparticle uptake: the phagocyte problem. Nano Today *10*, 487–510.

33. Huotari, J., and Helenius, A. (2011). Endosome maturation. EMBO J. *30*, 3481–3500.

34. Serfass, J.M., Takahashi, Y., Zhou, Z., Kawasawa, Y.I., Liu, Y., Tsotakos, N., Young, M.M., Tang, Z., Yang, L., Atkinson, J.M., et al. (2017). Endophilin B2 facilitates endosome maturation in response to growth factor stimulation, autophagy induction, and influenza A virus infection. J. Biol. Chem. *292*, 10097–10111.

35. Law, F., Seo, J.H., Wang, Z., DeLeon, J.L., Bolis, Y., Brown, A., Zong, W.X., Du, G., and Rocheleau, C.E. (2017). The VPS34 PI3K negatively regulates RAB-5 during endosome maturation. J. Cell Sci. *130*, 2007–2017.

36. Mi, J., Ray, P., Liu, J., Kuan, C.T., Xu, J., Hsu, D., Sullenger, B.A., White, R.R., and Clary, B.M. (2016). In vivo selection against human colorectal cancer xenografts identifies an aptamer that targets RNA helicase protein DHX9. Mol. Ther. Nucleic Acids *5*, e315.

37. Mi, J., Liu, Y., Rabbani, Z.N., Yang, Z., Urban, J.H., Sullenger, B.A., and Clary, B.M. (2010). In vivo selection of tumor-targeting RNA motifs. Nat. Chem. Biol. *6*, 22–24.

38. Burattini, S., Ferri, P., Battistelli, M., Curci, R., Luchetti, F., and Falcieri, E. (2004). C2C12 murine myoblasts as a model of skeletal muscle development: morpho-functional characterization. Eur. J. Histochem. *48*, 223–233.

39. Balci, B., and Dinçer, P. (2009). Efficient transfection of mouse-derived C2C12 myoblasts using a matrigel basement membrane matrix. Biotechnol. J. *4*, 1042–1045.

40. Neuhuber, B., Huang, D.I., Daniels, M.P., and Torgan, C.E. (2002). High efficiency transfection of primary skeletal muscle cells with lipid-based reagents. Muscle Nerve *26*, 136–140.

41. Goyenvalle, A., Griffith, G., Babbs, A., El Andaloussi, S., Ezzat, K., Avril, A., Dugovic, B., Chaussenot, R., Ferry, A., Voit, T., et al. (2015). Functional correction in mouse models of muscular dystrophy using exon-skipping tricyclo-DNA oligomers. Nat. Med. *21*, 270–275.

42. Yu, B., Zhao, X., Lee, L.J., and Lee, R.J. (2009). Targeted delivery systems for oligonucleotide therapeutics. AAPS J. *11*, 195–203.

43. Legiewicz, M., Lozupone, C., Knight, R., and Yarus, M. (2005). Size, constant sequences, and optimal selection. RNA *11*, 1701–1709.

44. Giangrande, P.H., Zhang, J., Tanner, A., Eckhart, A.D., Rempel, R.E., Andrechek, E.R., Layzer, J.M., Keys, J.R., Hagen, P.O., Nevins, J.R., et al. (2007). Distinct roles of E2F proteins in vascular smooth muscle cell proliferation and intimal hyperplasia. Proc. Natl. Acad. Sci. USA *104*, 12988–12993.

45. Dollins, C.M., Nair, S., Boczkowski, D., Lee, J., Layzer, J.M., Gilboa, E., and Sullenger, B.A. (2008). Assembling OX40 aptamers on a molecular scaffold to create a receptor-activating aptamer. Chem. Biol. *15*, 675–682.

46. McNamara, J.O., Kolonias, D., Pastor, F., Mittler, R.S., Chen, L., Giangrande, P.H., Sullenger, B., and Gilboa, E. (2008). Multivalent 4-1BB binding aptamers costimulate CD8+ T cells and inhibit tumor growth in mice. J. Clin. Invest. *118*, 376–386.

47. Mi, Z., Guo, H., Russell, M.B., Liu, Y., Sullenger, B.A., and Kuo, P.C. (2009). RNA aptamer blockade of osteopontin inhibits growth and metastasis of MDA-MB231 breast cancer cells. Mol. Ther. *17*, 153–161.

48. Daniels, D.A., Chen, H., Hicke, B.J., Swiderek, K.M., and Gold, L. (2003). A tenascin-C aptamer identified by tumor cell SELEX: systematic evolution of ligands by exponential enrichment. Proc. Natl. Acad. Sci. USA *100*, 15416–15421.

49. Shangguan, D., Meng, L., Cao, Z.C., Xiao, Z., Fang, X., Li, Y., Cardona, D., Witek, R.P., Liu, C., and Tan, W. (2008). Identification of liver cancer-specific aptamers using whole live cells. Anal. Chem. *80*, 721–728.

50. Chen, F., Zhou, J., Luo, F., Mohammed, A.B., and Zhang, X.L. (2007). Aptamer from whole-bacterium SELEX as new therapeutic reagent against virulent Mycobacterium tuberculosis. Biochem. Biophys. Res. Commun. *357*, 743–748.

51. Thiel, W.H., Bair, T., Peek, A.S., Liu, X., Dassie, J., Stockdale, K.R., Behlke, M.A., Miller, F.J., Jr., and Giangrande, P.H. (2012). Rapid identification of cell-specific, internalizing RNA aptamers with bioinformatics analyses of a cell-based aptamer selection. PLoS ONE *7*, e43836.

52. Gourronc, F.A., Rockey, W.M., Thiel, W.H., Giangrande, P.H., and Klingelhutz, A.J. (2013). Identification of RNA aptamers that internalize into HPV-16 E6/E7 transformed tonsillar epithelial cells. Virology *446*, 325–333.

53. Doshi, N., and Mitragotri, S. (2010). Macrophages recognize size and shape of their targets. PLoS ONE *5*, e10051.

54. Orava, E.W., Cicmil, N., and Gariépy, J. (2010). Delivering cargoes into cancer cells using DNA aptamers targeting internalized surface portals. Biochim. Biophys. Acta *1798*, 2190–2200.

55. Zhou, J., Swiderski, P., Li, H., Zhang, J., Neff, C.P., Akkina, R., and Rossi, J.J. (2009). Selection, characterization and application of new RNA HIV gp 120 aptamers for facile delivery of Dicer substrate siRNAs into HIV infected cells. Nucleic Acids Res. *37*, 3094–3109.

56. Zhou, J., Li, H., Li, S., Zaia, J., and Rossi, J.J. (2008). Novel dual inhibitory function aptamer-siRNA delivery system for HIV-1 therapy. Mol. Ther. *16*, 1481–1489.

57. Dassie, J.P., Liu, X.Y., Thomas, G.S., Whitaker, R.M., Thiel, K.W., Stockdale, K.R., Meyerholz, D.K., McCaffrey, A.P., McNamara, J.O., 2nd, and Giangrande, P.H. (2009). Systemic administration of optimized aptamer-siRNA chimeras promotes regression of PSMA-expressing tumors. Nat. Biotechnol. *27*, 839–849.

58. Tawiah, K.D., Porciani, D., and Burke, D.H. (2017). Toward the selection of cell targeting aptamers with extended biological functionalities to facilitate endosomal escape of cargoes. Biomedicines *5*, E51.

59. Wilson, J.M., de Hoop, M., Zorzi, N., Toh, B.H., Dotti, C.G., and Parton, R.G. (2000). EEA1, a tethering protein of the early sorting endosome, shows a polarized distribution in hippocampal neurons, epithelial cells, and fibroblasts. Mol. Biol. Cell *11*, 2657–2671.

60. Dickey, D.D., Dassie, J.P., and Giangrande, P.H. (2016). Method for Confirming Cytoplasmic Delivery of RNA Aptamers. In SiRNA Delivery Methods. Methods in Molecular Biology, *Volume 1364*, K. Shum and J. Rossi, eds (Humana Press), pp. 209–217.

61. Hernandez, L.I., Flenker, K.S., Hernandez, F.J., Klingelhutz, A.J., McNamara, J.O., and Giangrande, P.H. (2013). Methods for evaluating cell-specific, cell-internalizing RNA aptamers. Pharmaceuticals (Basel) *6*, 295–319.

62. van der Aa, M.A., Huth, U.S., Häfele, S.Y., Schubert, R., Oosting, R.S., Mastrobattista, E., Hennink, W.E., Peschka-Süss, R., Koning, G.A., and Crommelin, D.J. (2007). Cellular uptake of cationic polymer-DNA complexes via caveolae plays a pivotal role in gene transfection in COS-7 cells. Pharm. Res. *24*, 1590–1598.

63. Ohuchi, S. (2012). Cell-SELEX technology. Biores. Open Access *1*, 265–272.

64. Ye, M., Hu, J., Peng, M., Liu, J., Liu, J., Liu, H., Zhao, X., and Tan, W. (2012). Generating aptamers by cell-SELEX for applications in molecular medicine. Int. J. Mol. Sci. *13*, 3341–3353.

65. Lu, Q.L., Rabinowitz, A., Chen, Y.C., Yokota, T., Yin, H., Alter, J., Jadoon, A., Bou-Gharios, G., and Partridge, T. (2005). Systemic delivery of antisense oligoribonucleotide restores dystrophin expression in body-wide skeletal muscles. Proc. Natl. Acad. Sci. USA *102*, 198–203.

66. Lu, Q.L., Mann, C.J., Lou, F., Bou-Gharios, G., Morris, G.E., Xue, S.A., Fletcher, S., Partridge, T.A., and Wilton, S.D. (2003). Functional amounts of dystrophin produced by skipping the mutated exon in the mdx dystrophic mouse. Nat. Med. *9*, 1009–1014.

67. Heemskerk, H., de Winter, C., van Kuik, P., Heuvelmans, N., Sabatelli, P., Rimessi, P., Braghetta, P., van Ommen, G.J., de Kimpe, S., Ferlini, A., et al. (2010). Preclinical PK and PD studies on 2′-O-methyl-phosphorothioate RNA antisense oligonucleotides in the mdx mouse model. Mol. Ther. *18*, 1210–1217.

68. McMahon, J.M., and Wells, D.J. (2004). Electroporation for gene transfer to skeletal muscles: current status. BioDrugs *18*, 155–165.

69. Wolff, J.A., Malone, R.W., Williams, P., Chong, W., Acsadi, G., Jani, A., and Felgner, P.L. (1990). Direct gene transfer into mouse muscle in vivo. Science *247* (Pt 1), 1465–1468.

70. McMahon, J.M., Signori, E., Wells, K.E., Fazio, V.M., and Wells, D.J. (2001). Optimisation of electrotransfer of plasmid into skeletal muscle by pretreatment with hyaluronidase—increased expression with reduced muscle damage. Gene Ther. *8*, 1264–1270.

71. Favre, D., Cherel, Y., Provost, N., Blouin, V., Ferry, N., Moullier, P., and Salvetti, A. (2000). Hyaluronidase enhances recombinant adeno-associated virus (rAAV)-mediated gene transfer in the rat skeletal muscle. Gene Ther. *7*, 1417–1420.

72. Fromes, Y., Salmon, A., Wang, X., Collin, H., Rouche, A., Hagège, A., Schwartz, K., and Fiszman, M.Y. (1999). Gene delivery to the myocardium by intrapericardial injection. Gene Ther. *6*, 683–688.

73. Bolhassani, A., Mohit, E., Ghasemi, N., Salehi, M., Taghikhani, M., and Rafati, S. (2011). Enhancement of potent immune responses to HPV16 E7 antigen by using different vaccine modalities. BMC Proc. *5* (*Suppl 1*), P19.

74. Wojtkowiak-Szlachcic, A., Taylor, K., Stepniak-Konieczna, E., Sznajder, L.J., Mykowska, A., Sroka, J., Thornton, C.A., and Sobczak, K. (2015). Short antisense-locked nucleic acids (all-LNAs) correct alternative splicing abnormalities in myotonic dystrophy. Nucleic Acids Res. *43*, 3318–3331.

75. Feldherr, C.M., and Akin, D. (1997). The location of the transport gate in the nuclear pore complex. J. Cell Sci. *110*, 3065–3070.

76. Keminer, O., and Peters, R. (1999). Permeability of single nuclear pores. Biophys. J. *77*, 217–228.

77. González-Barriga, A., Kranzen, J., Croes, H.J., Bijl, S., van den Broek, W.J., van Kessel, I.D., van Engelen, B.G., van Deutekom, J.C., Wieringa, B., Mulders, S.A., and Wansink, D.G. (2015). Cell membrane integrity in myotonic dystrophy type 1: implications for therapy. PLoS ONE *10*, e0121556.

78. Chau, A., and Kalsotra, A. (2015). Developmental insights into the pathology of and therapeutic strategies for DM1: back to the basics. Dev. Dyn. *244*, 377–390.

79. Mulders, S.A., van den Broek, W.J., Wheeler, T.M., Croes, H.J., van Kuik-Romeijn, P., de Kimpe, S.J., Furling, D., Platenburg, G.J., Gourdon, G., Thornton, C.A., et al. (2009). Triplet-repeat oligonucleotide-mediated reversal of RNA toxicity in myotonic dystrophy. Proc. Natl. Acad. Sci. USA *106*, 13915–13920.

80. Lu, Q.L., and Wu, B. (2012). Systemic delivery of antisense oligomer in animal models and its implications for treating DMD. Methods Mol. Biol. *867*, 393–405.

81. Yokota, T., Lu, Q.L., Partridge, T., Kobayashi, M., Nakamura, A., Takeda, S., and Hoffman, E. (2009). Efficacy of systemic morpholino exon-skipping in Duchenne dystrophy dogs. Ann. Neurol. *65*, 667–676.

82. Renneberg, D., Bouliong, E., Reber, U., Schümperli, D., and Leumann, C.J. (2002). Antisense properties of tricyclo-DNA. Nucleic Acids Res. *30*, 2751–2757.

83. Zhou, J., and Rossi, J.J. (2010). Aptamer-targeted cell-specific RNA interference. Silence *1*, 4.

84. Rockey, W.M., Hernandez, F.J., Huang, S.Y., Cao, S., Howell, C.A., Thomas, G.S., Liu, X.Y., Lapteva, N., Spencer, D.M., McNamara, J.O., et al. (2011). Rational truncation of an RNA aptamer to prostate-specific membrane antigen using computational structural modeling. Nucleic Acid Ther. *21*, 299–314.

85. Wang, Y., Su, H.H., Yang, Y., Hu, Y., Zhang, L., Blancafort, P., and Huang, L. (2013). Systemic delivery of modified mRNA encoding herpes simplex virus 1 thymidine kinase for targeted cancer gene therapy. Mol. Ther. *21*, 358–367.

86. Kormann, M.S., Hasenpusch, G., Aneja, M.K., Nica, G., Flemmer, A.W., Herber-Jonat, S., Huppmann, M., Mays, L.E., Illenyi, M., Schams, A., et al. (2011). Expression of therapeutic proteins after delivery of chemically modified mRNA in mice. Nat. Biotechnol. *29*, 154–157.

87. Lupold, S.E., Hicke, B.J., Lin, Y., and Coffey, D.S. (2002). Identification and characterization of nuclease-stabilized RNA molecules that bind human prostate cancer cells via the prostate-specific membrane antigen. Cancer Res. *62*, 4029–4033.

88. Sambrook, J., and Russell, D.W. (2006). Purification of nucleic acids by extraction with phenol:chloroform. CSH Protoc. *2006*, pdb.prot4455.

89. Yan, A., and Levy, M. (2014). Cell internalization SELEX: in vitro selection for molecules that internalize into cells. Methods Mol. Biol. *1103*, 241–265.

90. Livak, K.J., and Schmittgen, T.D. (2001). Analysis of relative gene expression data using real-time quantitative PCR and the 2(-Delta Delta C(T)) method. Methods *25*, 402–408.

91. Ortuste Quiroga, H.P., Goto, K., and Zammit, P.S. (2016). Isolation, cryosection and immunostaining of skeletal muscle. Methods Mol. Biol. *1460*, 85–100.

92. Szeto, K., Latulippe, D.R., Ozer, A., Pagano, J.M., White, B.S., Shalloway, D., Lis, J.T., and Craighead, H.G. (2013). RAPID-SELEX for RNA aptamers. PLoS ONE *8*, e82667.